International Journal of Nanomedicine

Dovepress
open access to scientific and medical research

Open Access Full Text Article

ORIGINAL RESEARCH

Magnesium-doped Nanostructured Titanium Surface Modulates Macrophage-mediated Inflammatory Response for Ameliorative Osseointegration

This article was published in the following Dove Press journal:
International Journal of Nanomedicine

Xinrui Qiao
Jie Yang
Yuli Shang
Shu Deng
Shiyu Yao
Zhe Wang
Yi Guo
Cheng Peng

Department of Stomatology, The Second Hospital of Tianjin Medical University, Tianjin, People's Republic of China

Background: Next generation of coating materials on the surface of implants is designed with a paradigm shift from an inert material to an osteoimmunomodulatory material. Regulating immune response to biomedical implants through influencing the polarization of macrophage has been proven to be an effective strategy.

Methods: Through anodization and hydrothermal treatment, magnesium ion incorporated TiO_2 nanotube array (MgN) coating was fabricated on the surface of titanium and it is hypothesized that it has osteoimmunomodulatory properties. To verify this assumption, systematic studies were carried out by in vitro and in vivo experiments.

Results: Mg ion release behavior results showed that MgN coating was successfully fabricated on the surface of titanium using anodization and hydrothermal technology. Scanning electron microscopy (SEM) images showed the morphology of the MgN coating on the titanium. The expression of inflammation-related genes *(IL-6, IL-1β, TNF-α*) was downregulated in MgN group compared with TiO_2 nanotube (NT) and blank Ti groups, but anti-inflammatory genes (*IL-10* and *IL-1ra*) were remarkably upregulated in the MgN group. The in vitro and in vivo results demonstrated that MgN coating influenced macrophage polarization toward the M2 phenotype compared with NT and blank-Ti groups, which enhanced osteogenic differentiation of rat bone mesenchymal stem cells rBMSCs in conditioned media (CM) generated by macrophages.

Conclusion: MgN coating on the titanium endowed the surface with immune-regulatory features and exerted an advantageous effect on osteogenesis, thereby providing excellent strategies for the surface modification of biomedical implants.

Keywords: TiO_2 nanotube, magnesium ions, osteoimmunomodulation, macrophage

Introduction

It was widely recognized that titanium (Ti) and its alloys could be applied to dental and orthopedic implants. The insufficiency between the extraneous implant surface and the bone remains unsolved. In order to successfully install the implants, researchers make efforts to create bioactive coating materials on titanium surface using different techniques.[1,2] In these studies, favorable osteogenic, angiogenic and antibacterial capacities of coating materials have been widely explored.[3,4] However, many coating materials with excellent properties mentioned above could not achieve satisfactory results in the subsequent in vivo studies in terms of the regeneration of bones.[5,6] This inconsistency may be attributed to the ignored function of the immune cells which arrive at the implant–host interface before the osteoblastic cells and affect the in vivo fate of the implants.[7]

Correspondence: Cheng Peng
Department of Stomotology,
The Second Hospital of Tianjin Medical University, 23 Pingjiang Road, Hexi District, Tianjin 300211, People's Republic of China
Tel +86 139 2007 9346
Email peng_cheng2013@163.com

submit your manuscript | www.dovepress.com
DovePress
http://doi.org/10.2147/IJN.S239550

With the progress in understanding the reactions between the implant and host tissues, researchers began to realize that the responses of the immune system exert a profound impact on the osteogenesis stimulated by biomaterials. The cells from the immune system play an active part in bone dynamic activities via numerous transcription factors, cytokines, signalling molecules, and receptors.[8] Thus, the concept of osteoimmunology has been proposed and changed the design paradigm of biomaterial implants, from inert materials to implants with immunomodulatory function.[9,10] Optimal osteoimmunomodulatory properties facilitate an immune response to balance the osteogenesis and osteoclastogenesis that favors the regeneration of bone tissues.[11] In previous studies, cells in the osteoblastic lineage are often applied as the only choices to assess the effect of osteogenesis in cell experiments when developing novel implant biomaterials.[12] Since immune cells play such an essential part in the regeneration of bone tissues, a novel evaluation system involving both immune cells and bone cells is required to be constructed aiming to develop optimal implant biomaterials.

Of all cells in the immune system, macrophages, which are innate immune cells, play an important part in the immune responses induced by materials. Macrophages participate in the process of bone physiology and secrete some important regulatory molecules to influence bone remodeling.[13,14] Biomaterial implants induce polarization of macrophages towards different phenotypes, M1 and M2. M1 is a kind of pro-inflammatory macrophage, which could be "classically activated", and M2 is a kind of anti-inflammatory macrophage which could be "alternatively activated" in response to their microenvironment.[14,15] The interaction between polarization of macrophages and composition of biomaterials significantly influences the bone regeneration.[16] Therefore, macrophages can be utilized as a cellular model to evaluate the osteogenesis process with implanted biomaterials in vitro.

Development in osteoimmunology investigation has gained a common view that the surface morphology and chemistry of implant materials, especially nanotopography, can directly modulate the macrophage response.[17,18] Recent studies have found that nanotopography could facilitate macrophage functions, including adhesion, proliferation, differentiation and the secretion of inflammatory cytokines.[19–21] Hence, a significant portion of the current implant materials research has now started to explore various surface modification strategies to fine tune the immune system, either to eliminate the unwanted inflammation or to reprogram the immune cells to contribute to the osteogenesis process.

Nanostructured materials have a wide range of applications in biomedicine, and can be used to improve the surface biological activity of materials, cancer treatment, and biomarker detection.[22–25] Among the various biomimetic nanotopographical surfaces, microporous titanium dioxide (TiO_2) fabricated by simple electrochemical anodization, has been demonstrated to improve the healthy tissue biomaterial integration through regulating the expression of cellular signal molecules.[26] This nanoscaled topography mimics the microstructure of bone tissues to promote cellular activities.[27,28] Many nanostructured materials have drug-carrying capacity and large loading capacity.[23,29,30] The hollow and highly ordered TiO_2 nanotubes (NTs) were shown to form an ideal surface facilitating the release of functional substances, particularly the bioactive elements such as cytokines, growth factors, and inorganic ions.[31,32] Among them, inorganic element ions have been demonstrated to be extensively involved in bone tissue and many cellular functions. Xin et al have reported an effective method of implanting bioactive ions into the well-ordered NTs which are released at a low rate.[33] This strategy helped the surface architecture perform the functions of nanoscaled topography and inorganic ions. According to the design paradigm of the next generation, the foremost consideration for the surface design of implants is to construct multifunctional implants with surfaces which have osteogenesis properties and the ability of immunomodulation. Hence, the inorganic ions which are released at nanostructured surface on titanium implants stimulate immune responses and also promote osteogenesis.

Magnesium ions (Mg^{2+}) play essential roles in skeletal system, and their amount ranks fourth among all the elements in human body.[34] Magnesium ions are involved in bone metabolism by enhancing the differentiation and proliferation of osteoblastic cells.[35] Recently, accumulating research has discovered that Mg^{2+} fight against inflammation and are used in clinical practice. For example, Mg^{2+} are used to ameliorate seizure prophylaxis in obstetrics.[36] These results suggest that the cooperation of TiO_2 nanotubes and Mg ions may endow the surface of the implant with the properties of immunomodulation. In the previous study, Mg ions were doped in the TiO_2 NTs or other nanotopographic surfaces and tested to promote osseointegration using a conventional approach which focused on osteoblastic cells.[37,38] Nonetheless, in order to fully understand the mechanisms of nanostructure incorporated with Mg ions in the regeneration of bone tissues, it is far from enough

to just focus on the interactions within the cells of osteoblast lineage and biomaterials. The immune cells are required to be taken into account.

Accordingly, we fabricated a bioactive coating on the surface of titanium—Mg ions incorporated TiO_2 nanotubes (MgN), and it was hypothesized that it relatively conferred anti-inflammation effects and ameliorated host immune responses on the implants, which could ultimately promote the osteogenic properties on the Ti surface. To prove our assumption, systematic studies through biological assessments in vitro and histological evaluations in vivo were used to further explore the relation between immune responses and MgN coating, and also the influence of the microenvironment on immune system by MgN coating in osteogenesis.

Materials and Methods

Preparation of the Materials

Titanium plates with a size of 10×10×1 mm and cylindrical implants made of titanium (2×5 mm) were used. TiO_2 nanotubes were developed by electrochemical anodization. At room temperature, the platinum plate was used as the cathode, the titanium plate was used as the anode, and the electrolyte contained $NaHSO_4$, HF, and NaF. A constant potential was applied using a direct current (DC) power supply, with a voltage set at 12 V. The anodization time was 20 h. After electrochemical anodization, samples were ultrasonically cleaned in deionized water, and then dried in a vacuum drying oven for one hour (110°C). Samples of TiO_2 nanotubes were then cooled and treated by magnesium acetate solution with a concentration of 0.4 M for three hours at 200°C in autoclaves lined with Teflon to develop MgN coating via hydrothermal method. Before cell culture, all the specimens were sterilized using autoclaves. Smooth foil made of Ti was applied as the negative control in our experiments.[33,39]

Depiction of the Materials

The surface topography of the samples was observed with an electronic microscope for scanning (SEM, Hitachi S-4800, Japan). The amount of Mg^{2+} leached from TiO_2 nanotubes was detected via inductively coupled plasma atomic emission spectroscopy (ICP-AES). Multiple samples were infused in 10 mL of phosphate buffered saline (PBS) solution without stirring at 37°C for 7, 14 21, and 28 days, respectively. The number of Mg^{2+} released in the solutions mentioned above was detected by ICP-AES (Varian Liberty 150, USA). The contact angles between simulated body fluid (SBF) and various surfaces were measured by the optical contact angle apparatus (JC200D3, POWEACH Inc., China).

Cell Culture

We applied RAW 264.7 cells (RAW cell, a macrophage cell line) and rat bone mesenchymal stem cells (rBMSCs) (obtained from Cell Culture Center, Peking Union Medical College, China) in vitro study. Both kinds of cells were incubated at 37°C in a humidified CO_2 environment. Dulbecco's modified eagle medium (DMEM, Thermo Scientific, MA, USA) supplemented with 10% fetal bovine serum (FBS, Thermo Scientific) and 1% (v/v) penicillin/streptomycin (Invitrogen, Carlsbad, CA, USA) was used for cell culture. When the confluency was about 90%, RAW 264.7 cells were passaged via gentle scraping, while rBMSCs by trypsinization (Beyotime, China). The third to sixth passages of cells were utilized in the in vitro experiments.

Flow Cytometry

Flow cytometry analysis was applied to detect the surface markers of M1 (CCR7) and M2 (CD206) of macrophages. RAW264.7 cells were seeded on the surface of different samples in 24-well plates (1×10^4/well) and cultured for four days. Afterwards, they were scraped and collected. Samples were incubated with CCR7 (1:25) (GeneTex, Irvine, CA) and CD206 antibody (1:100) (AbD Serotec, Raleigh, NC) for 30 min at 4°C, followed by incubation with Dylight 488-antimouse and DyLight 405-antigoat secondary antibody (DAKO, Multilink, CA) for 30 min at 4°C. Then, the cells were washed with 1% BSA for three times and transferred into fluorescence activated cell sorting (FACS) tubes with 200 μL in each tube. Expressions of the surface markers in RAW264.7 cells were measured with flow cytometry (A50-Micro, UK).

The Expression of Inflammatory Genes

Raw274.6 cells were seeded on different samples at a density of 1×10^4/well. After four days of culture, the total RNA of cells was collected by using RNeasy Mini Kit (Qiagen, Germany). Total RNA (500 ng) was extracted for synthesizing the complementary DNA with the kit of PrimeScript cDNA synthesis (Qiagen, Germany) according to instructions of the manufacturer. The expression levels of the inflammation-related genes (*IL-1ra, IL-10, TNF-α, IL-1b, IL-6*) were

detected by reverse transcription-polymerase chain reaction (RT-PCR) assay, and the primers are shown in Table 1. *GAPDH* was choosen as the housekeeping gene in our study.

Enzyme-linked Immunosorbent Assay (ELISA)

The concentration of vascular endothelial growth factor (VEGF, pro-angiogenic) and bone morphogenetic protein-2 (BMP2, pro-osteogenic) in the culture medium of RAW264.7 cells was measured by ELISA assay (eBioscience, USA). After the samples were cultured for four days, the supernatants of RAW264.7 cells were obtained. The concentration of each factor mentioned above was measured at an absorbance of 450 nm with a microplate reader, and the standard curve was plotted.

Western Blot

Western blot was conducted to determine the expression levels of VEGF and BMP2. After being cultured for four days, RAW264.7 cells were lysed using lysis buffer. The protein levels were quantified with the bicinchoninic acid (BCA) kit (Thermo Scientific). Electrophoresis was conducted by the gel made of sodium dodecyl sulfate-polyacrylamide. Then, the proteins were transferred onto the nitrocellulose membranes. Afterwards, 5% (w/v) nonfat milk (dissolved in Tris-buffered saline (TBS)-Tween 20 buffer) was used to block the membranes for one hour. The membranes were co-incubated with specific primary antibodies, including β-actin, VEGF and BMP2 (1:1000; Servicebio, China) at 4°C overnight. On the next day, the membranes were washed with TBS-Tween 20 three times, and secondary antibodies conjugated with horseradish peroxidase were used for incubation at room temperature for one hour. After washing with TBS-Tween 20 three times, AlphaEaseFC (Alpha Innotech, San Leandro, CA, USA) was used to visualize the protein bands in darkness. Adobe Photoshop software was applied to quantify the intensity of the proteins.

Features of rBMSCs in Conditioned Medium (CM) on Multiple Surfaces

Collecting and Preparing CM

RAW264.7 cells were cultured in multiple samples prepared previously (blank Ti group, MgN group, NT group) in the 24-well plates with a concentration of 1×10^4 cells/well for 1– 14 days. The supernatant in each well was obtained and stored at 4°C in a refrigerator. The supernatant was diluted using DMEM (added 5% FBS) at a ratio of 1:1 for subsequent use.[40]

Proliferation Ability of rBMSCs in CM on Multiple Surfaces

rBMSCs (2×10^4 cells per well) were cultured on various samples (10×10×1 mm) in CM for 1, 3, 5, or 7 days, respectively. Cell Counting Kit-8 (CCK-8) (Beyotime, China) solution (10 μL) was added in each well, and the cells were incubated for 1–4 h in an incubator. The optical density (OD) values at 450 nm were measured for cell viability with a microplate reader.

Morphology of rBMSCs on Different Surfaces in CM

rBMSCs (2×10^4 cells per well) were cultured on various samples (10×10×1 mm) in CM for 1, 3, 5, or 7 days, respectively. Samples were fixed by formaldehyde (4%) for 30 minat room temperature, and washed with phosphate buffered saline (PBS) five times. Cells were added to the samples with 200 μL TRITC-labeled phalloidin working agent (Solarbio, China), and incubated for 30 min at room temperature in darkness. The samples were washed with PBS for three minutes, five times, and the nuclei were counterstained with 200 μL DAPI (Sigma, USA) solution (100 nmol) for 10 min. They were then rinsed three times with PBS. The samples were observed with a fluorescence microscope (the emission/excitation filter for

Table 1 Primers Used for Quantitative Reverse Transcription Polymerase Chain Reaction

Gene	Forward Primer Sequence (5–3)	Reverse Primer Sequence (5–3)
IL1ra	CTCCAGCTGGAGGAAGTTAAC	CTGACTCAAAGCTGGTGGTG
IL10	GAGAAGCATGGCCCAGAAATC	GAGAAATCGATGACAGCGCC
TNFα	CTGAACTTCGGGGTGATCGG	GGCTTGTCACTCGAATTTTGAGA
IL1β	TGGAGAGTGTGGATCCCAAG	GGTGCTGATGTACCAGTTGG
IL6	ATAGTCCTTCCTACCCCAATTTCC	GATGAATTGGATGGTCTTGGTCC
GAPDH	ATCCCATCACCATCTTCC	GAGTCCTTCCACGATACCA

TRITC: Em/Ex =570/540 nm, The emission/excitation filter for DAPI: Em/Ex=454/364 nm).

Osteogenesis Differentiation Process of rBMSCs on Different Surfaces

ALP Activity Assay

The rBMSCs (5×10^4cells/well) were cultured in CM for three and seven days, respectively, and alkaline phosphatase (ALP) was measured. Following PBS washing for three times, the cells were lysed by lysis buffer (2 mM NaCl, 10 mM Tris-HCl, and 1% Triton X-100, pH=7.5) and freeze–thaw cycle was repeated three times. Biochemical colorimetric test was used to determine the activity of ALP following instructions of the manufacturer (Solarbio, China). The activity of ALP was quantified at an absorbance of 510 nm.

Expressions of the Genes Related to Osteogenesis in CM Compared with Standard Medium

The rBMSCs (5×10^4cells/well) were cultured in CM or standard medium for seven days, respectively. Then the expressions of osteogenesis-associated genes runt-related transcription factor 2 (*RUNX2*), type I collagen (*COL1*), osteocalcin (*OCN*), ALP were measured. The results were standardized according to the *GAPDH* expression, which was a housekeeping gene. Total RNA was extracted from rBMSCs with the RNeasy Mini Kit (Qiagen). The extracted RNA was reversely transcript to obtain cDNA with a reverse transcription reagents kit (Takara, Japan) following instructions of the manufacturer. Real-time PCR assay was conducted with the Maxima SYBR-Ⅰ Green/ROX qPCR (Thermo Scientific) on a Rocha-LightCycler 96 (ABI7500 fast, Singapore). Gene expressions were calculated according to the method of $2^{-\Delta\Delta Ct}$. The sequences of the primers and the genes selected in this experiment are list in Table 2

The in vivo Experiments

Animal Experiments

The investigation conformed to the regulations of the experimental animal administration issued by the Ministry of Science and Technology of China (http://www.most.gov.cn), and the protocol was evaluated and accepted by the Institutional Ethics Committee of the Tianjin Medical University before the animal experiments. The specimens (cylinder, 2 mm in diameter and 5 mm in diameter, respectively) were cleaned by ultrasonic wave for five minutes before being autoclaved for 20 cycles at 121°C for 20 min. 21Twenty-one Wistar rats (10 weeks) were used in the experiment and randomly divided into three groups: blank Ti, NT, and MgN. All the rats were kept in a 12/12 hour day/night cycle room with air conditioner. Sterilized food and water were given per day and cages were changed weekly. The specimens were implanted into the tibia in each animal. Rats were euthanized at four weeks after operation, and the tibia samples were prepared for histological analysis.

Histology Analysis

The samples of bones with implants were fixed using formalin for 24 h at room temperature. Decalcified with 15% EDTA-2Na (Solarbio, China) until fine needle aspiration was conducted at the decalcification endpoint. After embedding in paraffin and fixed, the samples were sliced (vertical to the implants' long axis) into 4 μm sections. Afterwards, these sections were divided into four groups randomly for histological assessment. Tissue sections in Group 1 were stained with hematoxylin and eosin and observed under a microscope. Tissue sections in Group 2 were stained with Masson's Trichrome Stain Kit (Solarbio) to stain calcified bone (green) and muscle fibers (red), and observed under a transmitted light microscope. Immunofluorescent staining of tissue sections in groups 3 and 4 were performed to evaluate the level of CD206 and CCR7. After dewaxing and dehydration, primary antibodies for CCR7 (ab221209, AbCam) and CD206 (ab125028, AbCam) were used, and the sections were incubated at 37°C for one hour. Alexa Fluor® 488 (1:500, AbCam) or Cy3 with the conjugation of goat anti-rabbit IgG (1:100, AbCam) was applied as the secondary antibodies for CCR7and CD206, respectively. The tissues sections were incubated with the secondary antibodies for 30

Table 2 Primers sequences

Gene	Forward Primer Sequence (5–3)	Reverse Primer Sequence (5–3)
RUNX2	CGGACGAGGCAAGAGTTTCA	GGATGAGGAATGCGCCCTAA
COL1	GCAGACTGGCAACCTCAAGA	CAGGGCCAATGTCTAGTCCG
OCN	TAGTGAACAGACTCCGGCGCTA	TGTAGGCGGTCTTCAAGCCAT
Alp	TCATTCCCACGTTTTCACATTC	GTTGTTGTGAGCGTAATCTACC
GAPDH	ATCCCATCACCATCTTCC	GAGTCCTTCCACGATACCA

min at 37°C. Later, 4′-6-diamidino-2-phenylindole (DAPI) was utilized for the staining of nuclei. Then the laser confocal microscopy (Zeiss710, Germany) was used to obtain images.

Statistical Analysis

The results were described as average value ±standard deviation (SD). The data were analyzed with one-way analysis of variance (ANOVA) and Student's *t*-test. SPSS 17.0 software (SPSS 14.0, Chicago, IL, USA) was employed for statistical analysis. Differences between groups of $p<0.05$ were considered statistically significant, $p<0.01$ was considered highly significant.

Results

Specimen Depiction

Mg-incorporating TiO_2 nanotubes (MgN) were successfully fabricated on the surface of titanium using anodization and hydrothermal technology (Figure 1A). The surface morphology of samples detected by SEM is shown in Figure 1B. Well-ordered TiO_2 NTs with a diameter of approximately 100~200 nm were produced by anodization of the highly polished titanium plate (Figure 1B(i–ii)). To obtain MgN, the TiO_2 NT was subsequently hydrothermally treated in a Mg(Ac)2 solution, and the original nanostructure was retained while the diameter of the NTs decreased slightly (Figure 1B(iii–iv)). The release kinetic ability of Mg^{2+} was regulated by controlling the concentration of Mg^{2+} in the hydrothermal treatment procedure. As shown in Figure 1C, the release of Mg ions sustained in MgN group over 28 days. An initial Mg release burst phenomenon was seen in the plates within three days, and an equilibrium release was then achieved after three days. The angle of static contact measured by SBF showed the following trend: MgN< NT <blank Ti (Figure 1D). The angle of contact in the various stages of multilayers reduced dramatically from 89.25°±1.7° to 50.68°±1.6°.

In vitro Responses of RAW264.7 Cells

To explore the polarization of macrophages on the surface of different samples, RAW264.7 cells' polarization towards the phenotypes of M1 and M2 was detected by flow cytometry using CCR7 and CD206, respectively. The results suggested that RAW cells tended to express CD206, the M2 marker, in MgN group compared to NT and blank-Ti groups. Nonetheless, less RAW cells tended to express CCR7, the M1 marker, in the MgN group compared to the NT and blank-Ti groups. (Figure 2)

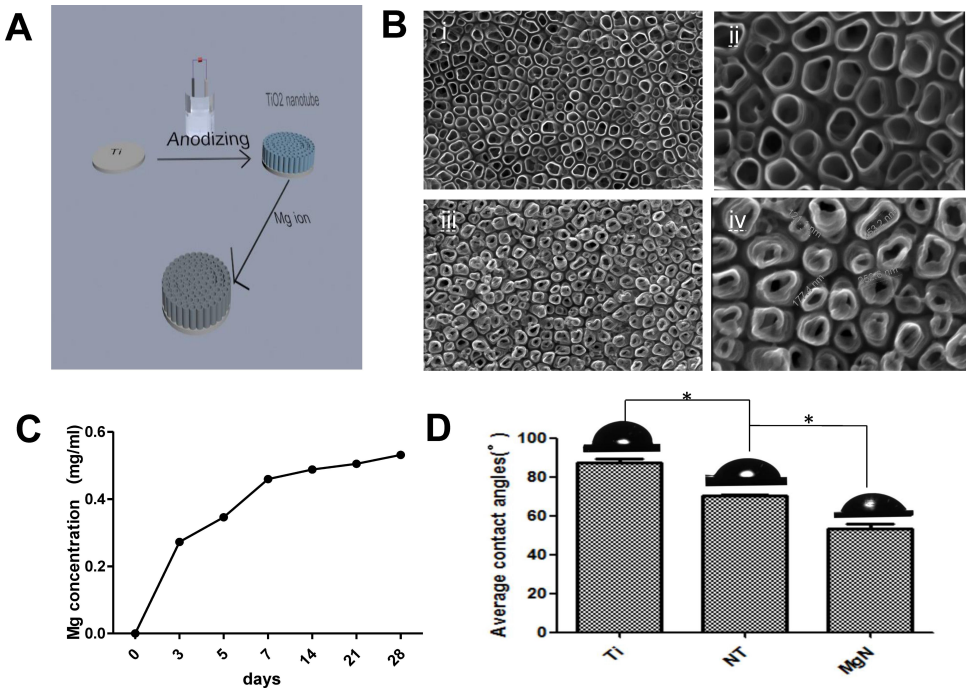

Figure 1 Surface characteristics.
Notes: (**A**) the process of fabricating MgN coating on the titanium. (**B**) SEM images of (i, ii) NT and (iii, iv) MgN coating on the titanium. (**C**) Release kinetics of Mg ion from MgN sample at day 3, 5, 7, 14, 21, and 28. (**D**) Contact angle of SBF on the surface of blank-Ti, NT and MgN samples. *p <0.05.
Abbreviations: MgN, magnesium ion incorporated TiO_2 nanotube arrays; NT, TiO_2 nanotube; SEM, scanning electron microscopy; SBF, simulated body fluid.

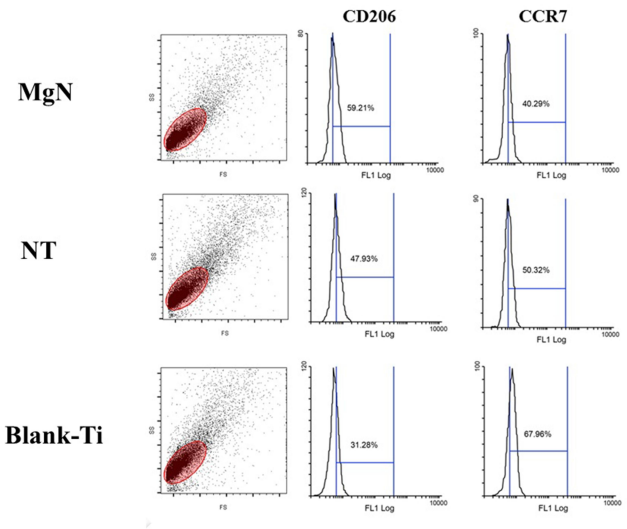

Figure 2 FACS results of RAW 264.7 cells cultured on different sample surfaces.
Notes: The mean fluorescence intensity of M2 marker (CD206) was increased after stimulated by MgN group compared with that by NT and blank-Ti groups; however, the mean fluorescence intensity of M1 marker (CCR7) declined under the same treatment.
Abbreviation: FACS, fluorescence activated cell sorting.

The phenotype of M1 secreted multiple inflammatory-related cytokines including tumor necrosis factor-α (TNF-α), interleukin-6 (IL-6) and interleukin-1β (IL-1β), however, M2 type generated interleukin-1ra (IL-1ra) and interleukin–10 (IL-10). The expression levels of these inflammatory genes were detected by RT-PCR. In comparison with NT and blank Ti groups, the IL-6, IL-1β and TNF-α were downregulated in the MgN group, but the genes with anti-inflammatory effects, such as IL-10 and IL-1ra, were remarkably upregulated in the MgN group (Figure 3A).

VEGF and BMP2 expressions in RAW264.7 cells were measured through ELISA and Western blotting. The results of ELISA showed that VEGF and BMP2 concentrations in the culture supernatant were higher in the MgN group compared with the NT and blank Ti groups (Figure 3C and D). The results of Western blot were consistent with those of ELISA (Figure 3B).

In vitro Responses of rBMSCs in Conditioned Medium (CM)

rBMSC Proliferation and Morphology on Different Surfaces in CM

The rBMSC proliferation was assessed by CCK-8 assay. The results revealed that the cell proliferation of rBMSCs on MgN

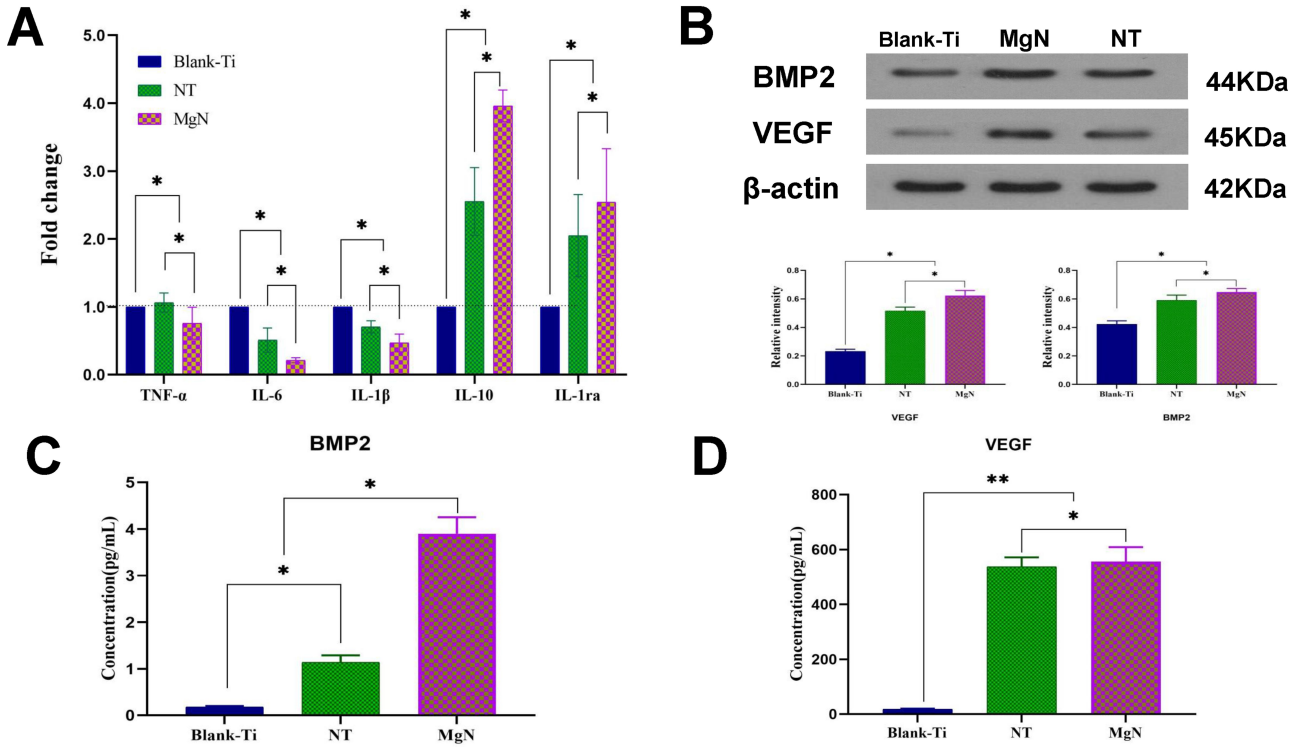

Figure 3 In vitro responses of RAW 264.7 cells cultured on different samples for four days. (**A**) The expression of inflammation-related genes TNF-α, IL-6, IL-1β, IL-10 and IL-1ra were detected by RT-PCR (blank-Ti group has been standardized as 1). (**B**) Western blotting analyses of VEGF and BMP2 respectively and their corresponding gray values. (**C, D**) ELISA determination of cytokines: (**C**) BMP2 (**D**) VEGF.
Notes: **denotes highly significant difference between groups; *denotes the statistically significant difference between groups; (*p <0.05, **p <0.01).
Abbreviations: TNF-α, tumor necrosis factor-α; IL-6, interleukin-6; IL-1β, interleukin-1β; IL-1ra, interleukin-1ra; IL-10, interleukin–10; VEGF, vascular endothelial growth factor; BMP2, bone morphogenetic protein 2; ELISA, enzyme-linked immunosorbent assay.

surfaces was significantly higher compared with the NT and blank Ti groups at the three specific time points (Figure 4A). The morphology of rBMSCs cultured in CM on different surfaces was evaluated after staining with DAPI and rhodamine-labeled phalloidine. The rBMSCs attached well and kept a normal shape on the three surfaces. Compared with NT and blank Ti groups, rBMSCs stretching on the MgN surfaces were facilitated to different degrees. (Figure 5).

Osteogenic Differentiation of rBMSCs on Different Surfaces in Standard Medium and CM

After rBMSCs were treated with or without the exposure to CM, the osteogenic features on different surfaces were assessed by determination of the expression of genes related to osteogenesis via RT-PCR analysis and ALP activity. The ALP activity of rBMSCs was remarkably upregulated on day seven following the stimulation by macrophage-conditioned MgN compared with the NT and blank Ti groups, and the difference was not significant between the NT and the blank Ti groups (Figure 4B). In CM or standard medium, osteogenic gene expression in culture supernatants showed the following trends: MgN> NT >blank Ti groups. However, the mRNA expressions of RUNX2 and OCN in rBMSCs were remarkably raised on day seven in the MgN group with macrophage-conditioned medium compared with standard medium. No significant difference was seen between the NT and blank Ti groups. Moreover, it was observed that the expression of ALP and *COL1* gene in rBMSCs on the NT and blank-Ti surface cultured in CM was downregulated on day seven compared with the rBMSCs cultured on standard medium but slightly upregulated on MgN surface (Figure 4C).

In vivo Study

To explore if the incorporation of Mg into TiO_2 NTs might affect the regeneration of bone tissues via changing the polarization of macrophages, an in vivo experiment was conducted to figure out the function of macrophages in the regeneration of bone tissue. The sections of the tissue were detected by CCR7 (M1; red) and CD206 (M2; red) immunofluorescent labelled staining with laser confocal microscopy. The CD206-positive and CCR7-positive sites are shown in Figures 6 and 7, respectively. The area of CCR7-positive sites was the smallest in MgN group and the largest in the NT and Ti groups (Figure 7). On the contrary, the area of

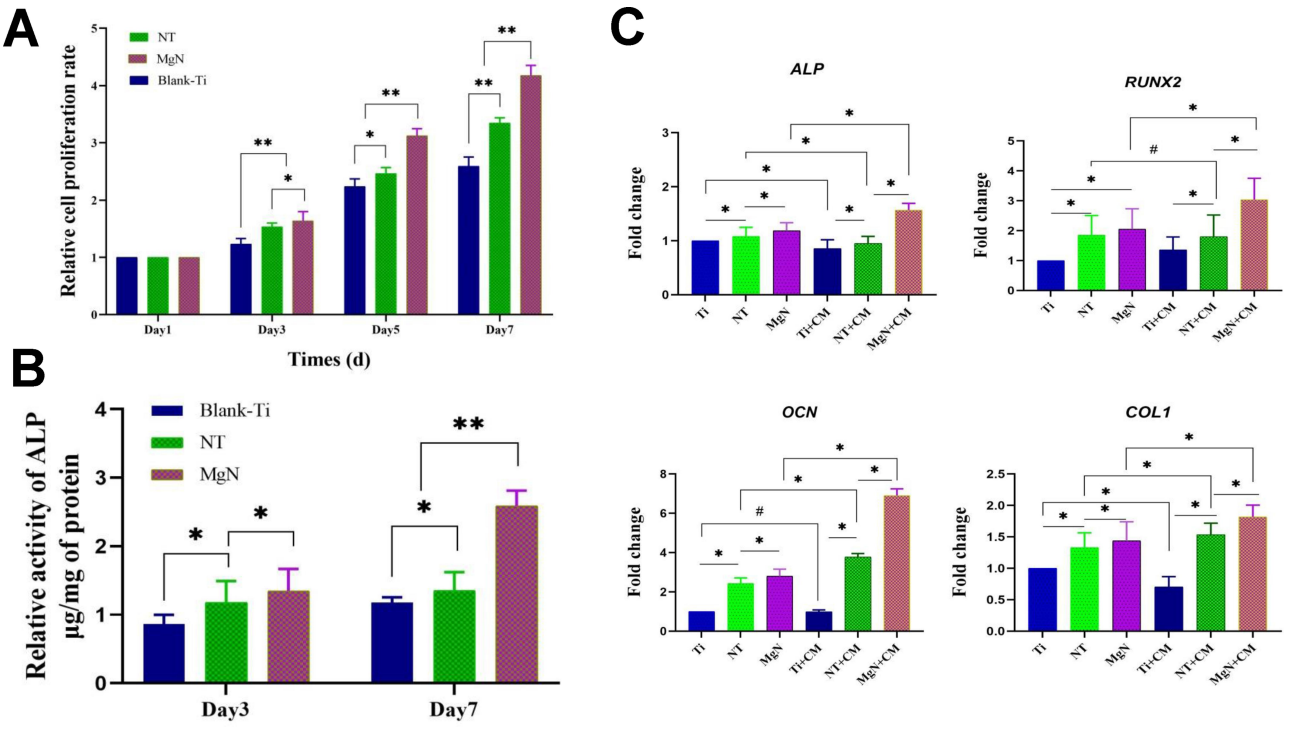

Figure 4 (**A**) Cell proliferation of rBMSCs cultured for one, three, five, and seven days in CM on various samples. (**B**) ALP activity of rBMSCs cultured for three and seven days in conditioned medium on various samples. (**C**) mRNA expression of osteogenic genes (ALP, RUNX2, OCN, COL1) of rBMSCs cultured on various samples in standard culture medium vs in CM after osteogenic induction for seven days.

Notes: *Statistically significant difference between groups (p <0.05); **highly significant difference between groups (p <0.01); #no significant difference between groups (p >0.05).

Abbreviations: rBMSCs, rat bone mesenchymal stem cells; RUNX2, runt-related transcription factor 2; COL1, type I collagen; OCN, osteocalcin; CM, conditioned medium.

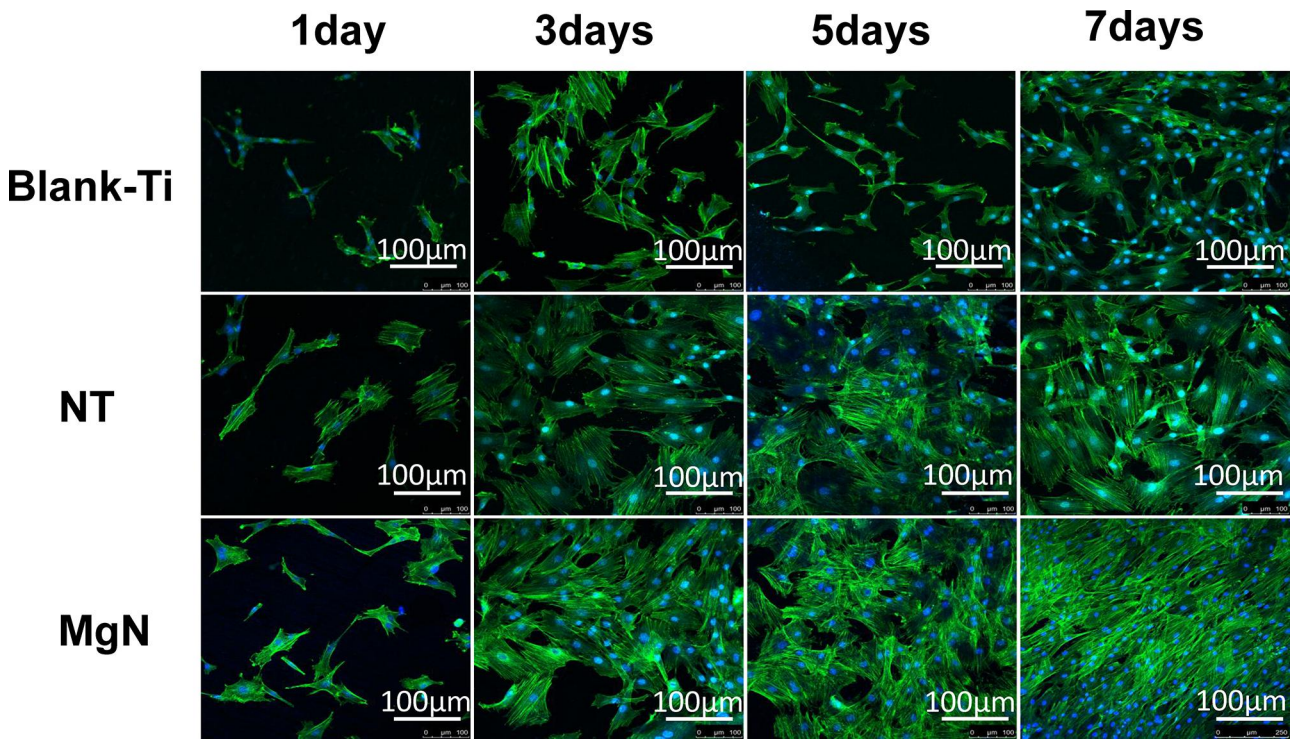

Figure 5 Morphology of rBMSCs on different surfaces of Ti, NT and MgN in CM by fluorescence microscopy.
Notes: The rBMSCs attached well and kept a normal shape on the three surfaces. Compared with NT and blank Ti groups, rBMSCs stretching on MgN surfaces were facilitated to different degrees.
Abbreviations: rBMSCs, rat bone mesenchymal stem cells; CM, conditioned medium.

CD206-positive sites was the smallest in the blank Ti and NT groups and the largest in the MgN group (Figure 6). The interface of bone implants was assessed with sections stained by H&E and Masson staining (Figure 8). Four weeks after implantation, cubic and short pre-osteoblasts were lined surrounding the trabecular bone and MgN implants. On the same day, newly generated small vessels were scattered in the trabecular bone. Angiogenesis and osteogenesis were intricately modulated in the formation of bone tissues. The MgN group showed robust new formation of bone tissue, which delimited the defected area with the implantation of MgN implant. The defected area filled by the blank Ti and NT groups showed less bone area than that of the MgN group, indicating that MgN could enhance the formation of bone tissues compared with the NT and blank-Ti group. Moreover, H&E staining showed more fibrillar connective tissue was found around the defect area filled by the NT and blank-Ti implants compared with the MgN implant.

Discussion

The ideal implants for dental use require multiple properties including excellent bioactivity, outstanding mechanical strength, and satisfactory biocompatibility.[41] With the progress in biological material design paradigms, the implant materials are required to regulate local immunity and promote the connection between the host and implants. The significant advantage of TiO_2 NTs is that it can be used as a good delivery platform including drugs (photocatalysis for cancer treatment), growth factors, and inorganic bioactive elements (Sr, Zn and Mg).[42,43] Therefore, it is necessary to fabricate a bioactive coating surface of the implant for favorable osteogenic activity and immunomodulatory effects. In this work, bioactive Mg-doped TiO_2 NTs are generated on Ti implants through anodic oxidation and hydrothermal treatment. The results suggest that the coating of titanium with MgN can influence macrophage polarization and induce a favorable immune environment for osteogenesis.

Macrophages are involved in the response of immune system to the implanted biomaterials. After implantation, macrophages rapidly migrate to the surface of implants and differentiate into different phenotypes (M1 or M2 phenotype) in response to the physicochemical properties of biomaterials.[44] M1 macrophages secrete numerous inflammatory-related cytokines (such as IL-6, IL-1β, TNF-α, etc), which increase the activity of osteoclasts and eventually

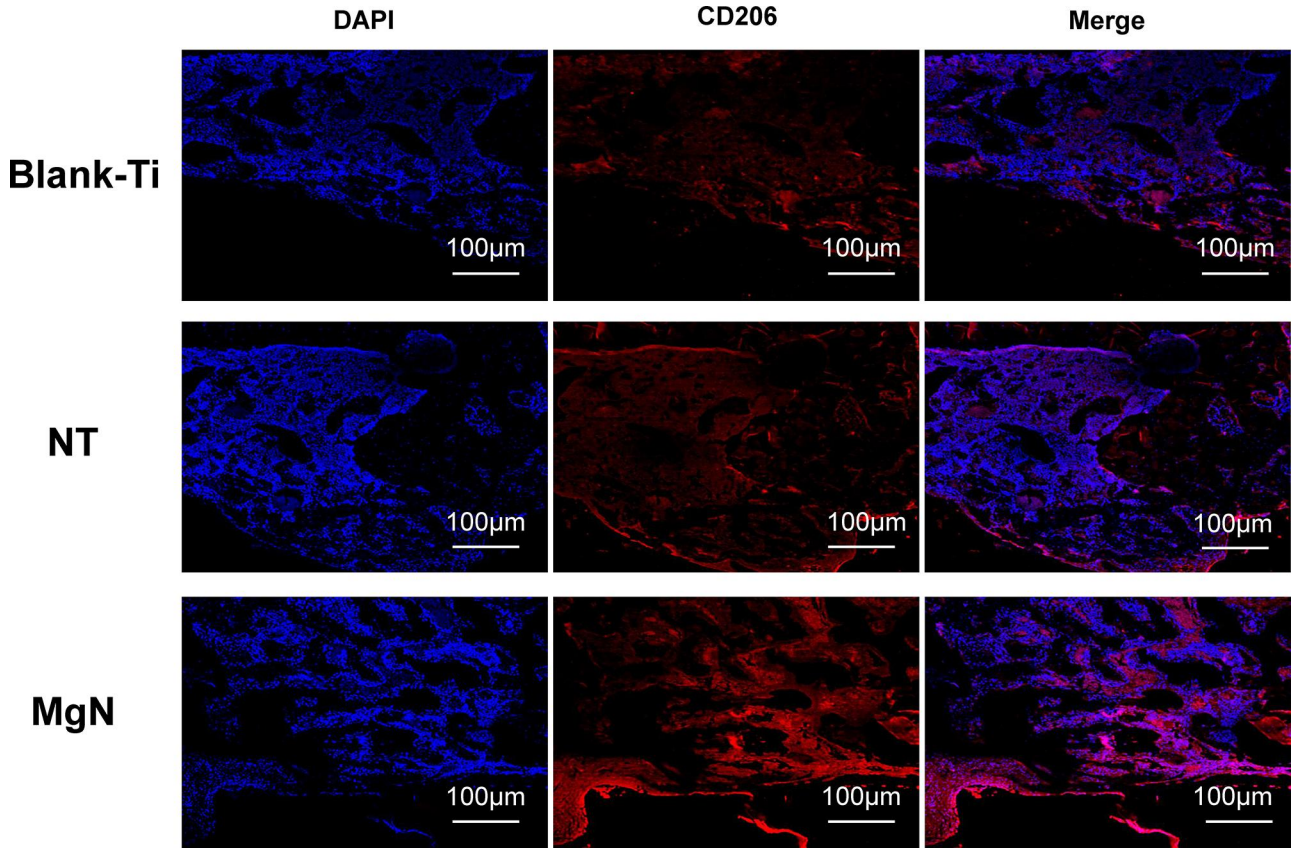

Figure 6 Detection of M2 marker (CD206) in tissue sections from rat bone by immunolabeling and confocal immunofluorescence imaging.
Notes: The area of CD206-positive sites (M2; red) was the smallest in blank Ti and NT groups and the largest in the MgN group.
Abbreviation: CD206, the surface markers M2 of macrophages.

lead to bone resorption. However, M2 macrophages are mainly involved in the mid-late stage of bone tissue regeneration and induce the bone formation by secreting vascular endothelial growth factor (VEGF), bone morphogenetic protein 2 (BMP-2) and other cytokines.[45,46]

An experimental model can be established when designing biomaterials of the implants. A beneficial immune status regulated by biomaterials could result in an enhanced osteogenesis activity. However, a harmful immune response may result in implant failure. Thus, systematic studies are required to assess the osteogenic ability and immune system participation of biomaterials of implants.[47] Compared with the NT group, MgN showed a satisfactory effect on switching the macrophage phenotype toward M2 type. After induction by MgN, fewer macrophages expressed CCR7 and more expressed CD206. Furthermore, after incubated on the surface of MgN, the inflammatory genes IL-6, TNF-α and IL1β were reduced, however, the expressions of genes related to anti-inflammation such as IL-10 and IL1ra were significantly increased in comparison with the NT and blank Ti groups. The results clearly indicated that macrophages were polarized to M2 type due to the stimulation of MgN. Based on the result of Mg ion release kinetics shown in Figure 1, the release of the Mg ions increased with time, but there was no Mg ion in the NT group. Some studies revealed that free Mg ions could reduce the production of inflammation-related cytokines through inhibiting the TLR receptor signaling pathway.[48] Other studies suggested that the incorporation of Mg in calcium phosphate could modulate the immune environment, in agreement with our results.[49] Therefore, it was speculated that suppressing the inflammation in MgN might result in Mg release. Moreover, the concentration of Mg ions which were applied as anti-inflammation factors in other studies was relatively high (60 mg/L).[50] The concentration was considered effective in clinical practice but also pretty close to its toxic dosage. Titanium dioxide NTs serve as an ideal carrier to deliver Mg locally. The Mg-incorporating TiO_2 nanotubes release magnesium ions in local areas at a fairly low level and hypermagnesemia is not a concern.

The results above support our hypothesis that incorporating Mg ion into TiO_2 NTs may be beneficial in the

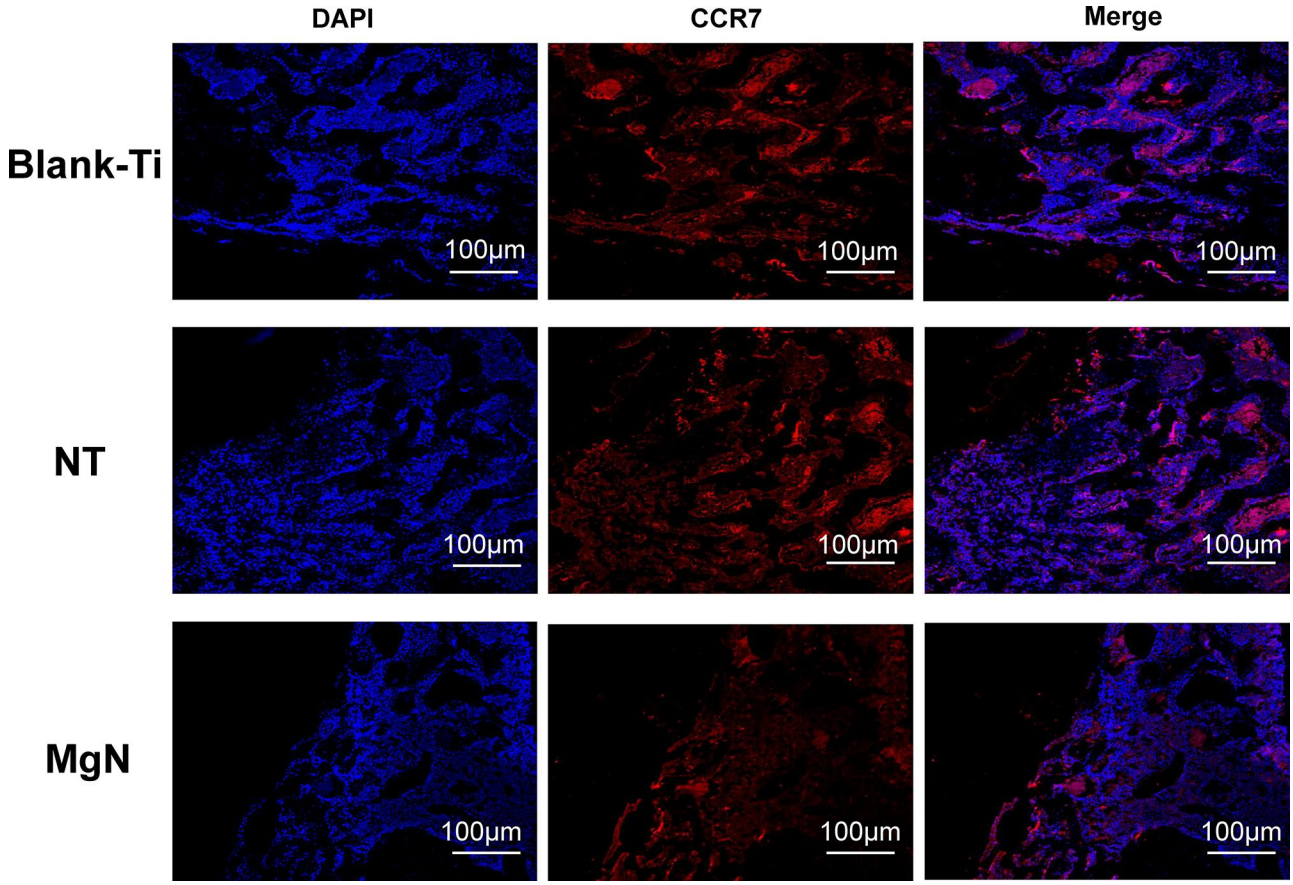

Figure 7 Detection of M1 marker (CCR7) in tissue sections from rat bone by immunolabeling and confocal immunofluorescence imaging.
Notes: The area of CCR7-positive sites (M1; red) was the smallest in MgN group and the largest in NT and Ti group.
Abbreviation: CCR7, the surface markers M1 of macrophages.

polarization of macrophages toward M2 type. The amount of M2 phenotype increased in MgN group, which contributed to the accumulation of the factors related to osteogenic growth including VEGF and BMP2. These two factors are known to promote wound healing and formation of bone tissues.[51,52] BMP2 is known as an essential member in the BMP family and also an ideal osteogenesis agent.[53] VEGF is an important pro-angiogenic protein which could bind with VEGFR to stimulate the downstream adaptors and promote angiogenesis.[54] MgN remarkably increased the gene expression of VEGF and BMP2 in macrophages, indicating that the variation of macrophage polarization could be the molecular mechanisms contributing to the osteogenesis influence of Mg. Further studies are required to investigate the underlying mechanisms of Mg affecting the polarization of macrophages and osteogenesis.

Most previous in vitro studies using the conventional "one-cell type" approach for evaluating the biocompatibility of materials have not precisely simulated the environment in vivo. Since the term "osteoimmunomodulation" was raised, researchers have focused on the important role of regulatory immune cells in generating a beneficial osteoimmune environment to improve the osseointegration ability of the implants.[55] To assess the influence of the cytokines generated by macrophages on multiple surfaces, we established a culture system in which rBMSCs were cultured in CM on the specific surfaces. The results suggested that MgN coating and corresponding CM worked together to facilitate the osteogenic process of rBMSCs. ALP, OCN, COL1 and RUNX2 are markers in osteoblast lineage.[56] A significant increase was found in the expression levels of genes related to osteogenesis in the MgN group with macrophage-conditioned medium compared with standard medium, while this increase was not obvious in NT and blank Ti groups and even the trend of suppression appeared. This result was likely because the bioactive proteins generated by macrophages were exposed on multiple surfaces. The available evidence has suggested that the immune environment

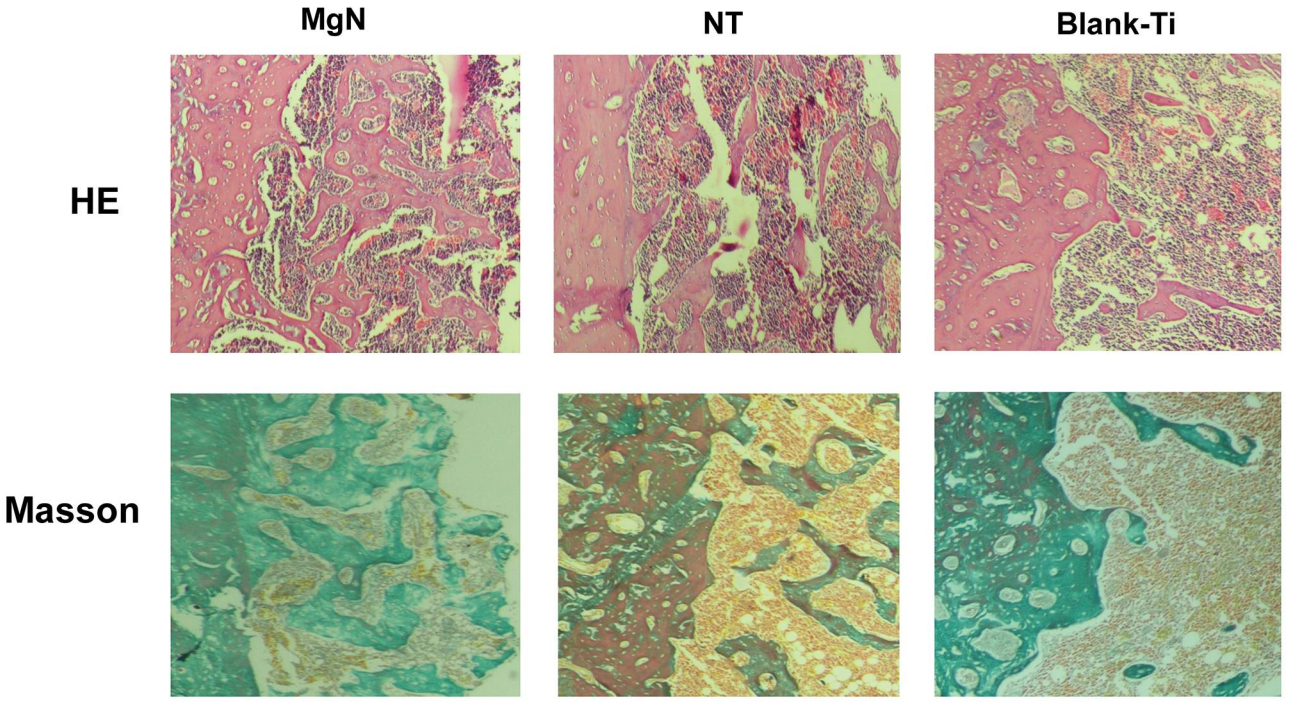

Figure 8 H&E staining and Masson's trichrome staining evaluation of the effects of MgN, NT and blank-Ti on bone regeneration.
Notes: Four weeks after implantation, cubic and short pre-osteoblasts were lined surrounding the trabecular bone and MgN implants. On the same day, newly generated small vessels were scattered in trabecular bone. Angiogenesis and osteogenesis were intricately modulated in the formation of bone tissues. The MgN group showed robust new formation of bone tissues, which delimited the defected area with the implantation of MgN implant. The defected area filled by the blank Ti and NT groups showed less bone area than that of MgN group, indicating that MgN could enhance the formation of bone tissues compared with the NT and blank-Ti groups.
Abbreviation: H&E staining, hematoxylin and eosin staining.

around the implant created by the coating of MgN improves osteogenesis. In addition, MgN promoted rBMSC proliferation and CM spreading compared with NT group, which may be attributed to higher hydrophilic surfaces of MgN. It has been reported that high hydrophilicity of the substrates can improve cell spreading, adhesion, and proliferation.[57]

The in vitro data showed that MgN manipulated macrophage polarization and enhanced osteoimmunomodulation. However, we have to point out that immune responses are complicated, and cannot be easily mimicked in in vitro experiments. Further in vivo experiments are required to prove the in vitro results. The immunofluorescence staining results of cells adhering to the sample surfaces indicated that MgN tended to induce the generation of M2 cells rather than M1 cells compared with the NT group. The histological results demonstrated that MgN contributed to a remarkable reduction in the amount of inflammation cells accumulating near the implant, and a higher proportion of M2 cells was indicated by immunohistochemistry. The interface of the bone implant was detected by H&E and Masson staining, and the results showed that the formation of bones was increasingly promoted by MgN compared with the NT group. The in vivo results were consistent with those of in vitro experiments. The data demonstrated that the MgN-treated titanium had an osteoimmunomodulatory effect on the polarization of macrophages.

The paradigm shift for developing implant materials emphasized the essential role of osteoimmunomodulation, which indicated that the features should be indispensable parameters in evaluating and developing the advanced implant biomaterials. In our research, osteo-immunomodulation was defined as the modulation of inflammation reaction with the implants and also the influence of immuno-microenvironments on the biological activities of bone marrow mesenchymal stem cells. In this study, the strategy of incorporating Mg into TiO_2 NTs was proven capable of modulating the immune reaction to enhance the regeneration of bone tissues. Our results will promote the development of immune-regulatory coatings which could enhance the osseointegration abilities of the orthopedic implants.

Conclusion

In this study, Mg-incorporated NT array (MgN) on the titanium implants was successfully prepared by hydrothermal treatment and anodization processes. MgN coating on the

titanium endowed the surface with immune-regulatory features and exerted an advantageous effect on the inhibition of the inflammation responses in macrophages. The in vivo and in vitro data suggested that MgN-loaded Ti surface showed excellent performance in osteoimmunomodulation and osteogenesis, thereby providing a potential choice for the surface regulation of biomaterial implants.

Funding

Xinrui Qiao and Jie Yang contributed equally to this work. This work was supported by the Tianjin Natural Science Foundation (Grant number 17JCYBJC26300) and Tianjin Natural Science Foundation (Grant number 18JCQN JC72100).

Disclosure

The authors report no conflicts of interest in this work.

References

1. Lu RJ, Wang X, He HX, et al. Tantalum-incorporated hydroxyapatite coating on titanium implants: its mechanical and in vitro osteogenic properties. *J Mater Sci Mater Med*. 2019;30(10):111. doi:10.1007/s10856-019-6308-9
2. Liu J, Yang W, Tao B, et al. Preparing and immobilizing antimicrobial osteogenic growth peptide on titanium substrate surface. *J Biomed Mater Res A*. 2018;106(12):3021–3033. doi:10.1002/jbm.a.36491
3. Yu Y, Jin G, Xue Y, Wang D, Liu X, Sun J. Multifunctions of dual Zn/Mg ion co-implanted titanium on osteogenesis, angiogenesis and bacteria inhibition for dental implants. *Acta Biomater*. 2017;49:590–603. doi:10.1016/j.actbio.2016.11.067
4. Jin G, Qin H, Cao H, et al. Synergistic effects of dual Zn/Ag ion implantation in osteogenic activity and antibacterial ability of titanium. *Biomaterials*. 2014;35(27):7699–7713. doi:10.1016/j.biomaterials.2014.05.074
5. Ghadami F, Saber-Samandari S, Rouhi G, et al. The effects of bone implants' coating mechanical properties on osseointegration: in vivo, in vitro, and histological investigations. *J Biomed Mater Res A*. 2018;106(10):2679–2691. doi:10.1002/jbm.a.36465
6. Zhao SF, Jiang QH, Peel S, Wang XX, He FM. Effects of magnesium-substituted nanohydroxyapatite coating on implant osseointegration. *Clin Oral Implants Res*. 2013;24(Suppl A100):34–41. doi:10.1111/j.1600-0501.2011.02362.x
7. Vishwakarma A, Bhise NS, Evangelista MB, et al. Engineering immunomodulatory biomaterials to tune the inflammatory response. *Trends Biotechnol*. 2016;34(6):470–482. doi:10.1016/j.tibtech.2016.03.009
8. Walsh MC, Kim N, Kadono Y, et al. Osteoimmunology: interplay between the immune system and bone metabolism. *Annu Rev Immunol*. 2006;24(1):33–63. doi:10.1146/annurev.immunol.24.021605.090646
9. Takayanagi H. Osteoimmunology: shared mechanisms and crosstalk between the immune and bone systems. *Nat Rev Immunol*. 2007;7(4):292–304. doi:10.1038/nri2062
10. Takayanagi H. Inflammatory bone destruction and osteoimmunology. *J Periodontal Res*. 2005;40(4):287–293. doi:10.1111/j.1600-0765.2005.00814.x
11. Kovach TK, Dighe AS, Lobo PI, Cui Q. Interactions between MSCs and immune cells: implications for bone healing. *J Immunol Res*. 2015;2015:752510. doi:10.1155/2015/752510
12. Mechiche Alami S, Gangloff SC, Laurent-Maquin D, Wang Y, Kerdjoudj H. Concise review: in vitro formation of bone-like nodules sheds light on the application of stem cells for bone regeneration. *Stem Cells Transl Med*. 2016;5(11):1587–1593. doi:10.5966/sctm.2015-0413
13. Schlundt C, El Khassawna T, Serra A, et al. Macrophages in bone fracture healing: their essential role in endochondral ossification. *Bone*. 2018;106:78–89. doi:10.1016/j.bone.2015.10.019
14. Mosser DM, Edwards JP. Exploring the full spectrum of macrophage activation. *Nat Rev Immunol*. 2008;8(12):958–969. doi:10.1038/nri2448
15. Mills CD, Kincaid K, Alt JM, Heilman MJ, Hill AM. M-1/M-2 macrophages and the Th1/Th2 paradigm. *J Immunol*. 2000;164(12):6166–6173. doi:10.4049/jimmunol.164.12.6166
16. Gordon S, Taylor PR. Monocyte and macrophage heterogeneity. *Nat Rev Immunol*. 2005;5(12):953–964. doi:10.1038/nri1733
17. Smith BS, Capellato P, Kelley S, Gonzalez-Juarrero M, Popat KC. Reduced in vitro immune response on titania nanotube arrays compared to titanium surface. *Biomater Sci*. 2013;1(3):322–332. doi:10.1039/C2BM00079B
18. Chen Z, Ni S, Han S, et al. Nanoporous microstructures mediate osteogenesis by modulating the osteo-immune response of macrophages. *Nanoscale*. 2017;9(2):706–718. doi:10.1039/C6NR06421C
19. Kim JY, Khang D, Lee JE, Webster TJ. Decreased macrophage density on carbon nanotube patterns on polycarbonate urethane. *J Biomed Mater Res A*. 2009;88(2):419–426. doi:10.1002/jbm.a.31799
20. Giavaresi G, Tschon M, Daly JH, et al. In vitro and in vivo response to nanotopographically-modified surfaces of poly(3-hydroxybutyrate-co-3-hydroxyvalerate) and polycaprolactone. *J Biomater Sci Polym Ed*. 2006;17(12):1405–1423. doi:10.1163/156856206778937226
21. Pujari S, Hoess A, Shen J, et al. Effects of nanoporous alumina on inflammatory cell response. *J Biomed Mater Res A*. 2014;102(11):3773–3780. doi:10.1002/jbm.a.35048
22. Xue T, Liang W, Li Y, et al. Ultrasensitive detection of miRNA with an antimonene-based surface plasmon resonance sensor. *Nat Commun*. 2019;10(1):28. doi:10.1038/s41467-018-07947-8
23. Tao W, Ji X, Zhu X, et al. Two-dimensional antimonene-based photonic nanomedicine for cancer theranostics. *Adv Mater*. 2018;30(38):e1802061. doi:10.1002/adma.201802061
24. Xing C, Chen S, Liang X, et al. Two-dimensional MXene (Ti3C2)-integrated cellulose hydrogels: toward smart three-dimensional network nanoplatforms exhibiting light-induced swelling and bimodal photothermal/chemotherapy anticancer activity. *ACS Appl Mater Interfaces*. 2018;10(33):27631–27643. doi:10.1021/acsami.8b08314
25. Tao W, Kong N, Ji X, et al. Emerging two-dimensional monoelemental materials (Xenes) for biomedical applications. *Chem Soc Rev*. 2019;48(11):2891–2912. doi:10.1039/C8CS00823J
26. Cheng Y, Yang H, Yang Y, et al. Progress in TiO2 nanotube coatings for biomedical applications: a review. *J Mater Chem B*. 2018;6(13):1862–1886. doi:10.1039/C8TB00149A
27. Indira K, Mudali UK, Rajendran N. In-vitro biocompatibility and corrosion resistance of strontium incorporated TiO2 nanotube arrays for orthopaedic applications. *J Biomater Appl*. 2014;29(1):113–129. doi:10.1177/0885328213516821
28. Aguirre R, Echeverry-Rendon M, Quintero D, et al. Formation of nanotubular TiO2 structures with varied surface characteristics for biomaterial applications. *J Biomed Mater Res A*. 2018;106(5):1341–1354. doi:10.1002/jbm.a.36331
29. Qiu M, Wang D, Liang W, et al. Novel concept of the smart NIR-light-controlled drug release of black phosphorus nanostructure for cancer therapy. *Proc Natl Acad Sci U S A*. 2018;115(3):501–506. doi:10.1073/pnas.1714421115

30. Sun Z, Zhao Y, Li Z, et al. TiL4 -coordinated black phosphorus quantum dots as an efficient contrast agent for in vivo photoacoustic imaging of cancer. *Small*. 2017;13(11).
31. Han CM, Jang TS, Kim HE, Koh YH. Creation of nanoporous TiO2 surface onto polyetheretherketone for effective immobilization and delivery of bone morphogenetic protein. *J Biomed Mater Res A*. 2014;102(3):793–800. doi:10.1002/jbm.a.34748
32. von Wilmowsky C, Bauer S, Roedl S, Neukam FW, Schmuki P, Schlegel KA. The diameter of anodic TiO2 nanotubes affects bone formation and correlates with the bone morphogenetic protein-2 expression in vivo. *Clin Oral Implants Res*. 2012;23(3):359–366. doi:10.1111/j.1600-0501.2010.02139.x
33. Xin Y, Jiang J, Huo K, Hu T, Chu PK. Bioactive SrTiO(3) nanotube arrays: strontium delivery platform on Ti-based osteoporotic bone implants. *ACS Nano*. 2009;3(10):3228–3234. doi:10.1021/nn9007675
34. Tsuboi S, Nakagaki H, Ishiguro K, et al. Magnesium distribution in human bone. *Calcif Tissue Int*. 1994;54(1):34–37. doi:10.1007/BF00316287
35. Wu L, Feyerabend F, Schilling AF, Willumeit-Romer R, Luthringer BJC. Effects of extracellular magnesium extract on the proliferation and differentiation of human osteoblasts and osteoclasts in coculture. *Acta Biomater*. 2015;27:294–304. doi:10.1016/j.actbio.2015.08.042
36. Sugimoto J, Romani AM, Valentin-Torres AM, et al. Magnesium decreases inflammatory cytokine production: a novel innate immunomodulatory mechanism. *J Immunol*. 2012;188(12):6338–6346. doi:10.4049/jimmunol.1101765
37. Cecchinato F, Xue Y, Karlsson J, et al. In vitro evaluation of human fetal osteoblast response to magnesium loaded mesoporous TiO2 coating. *J Biomed Mater Res A*. 2014;102(11):3862–3871. doi:10.1002/jbm.a.35062
38. Cecchinato F, Karlsson J, Ferroni L, et al. Osteogenic potential of human adipose-derived stromal cells on 3-dimensional mesoporous TiO2 coating with magnesium impregnation. *Mater Sci Eng C Mater Biol Appl*. 2015;52:225–234. doi:10.1016/j.msec.2015.03.026
39. Yan Y, Wei Y, Yang R, et al. Enhanced osteogenic differentiation of bone mesenchymal stem cells on magnesium-incorporated titania nanotube arrays. *Colloids Surf B Biointerfaces*. 2019;179:309–316. doi:10.1016/j.colsurfb.2019.04.013
40. Zhang W, Lu X, Yuan Z, et al. Establishing an osteoimmunomodulatory coating loaded with aspirin on the surface of titanium primed with phase-transited lysozyme. *Int J Nanomedicine*. 2019;14:977–991. doi:10.2147/IJN.S190766
41. Rasouli R, Barhoum A, Uludag H. A review of nanostructured surfaces and materials for dental implants: surface coating, patterning and functionalization for improved performance. *Biomater Sci*. 2018;6(6):1312–1338. doi:10.1039/C8BM00021B
42. Luo M, Fan T, Zhou Y, Zhang H, Mei L. 2D black phosphorus–based biomedical applications. *Adv Funct Mater*. 2019;29(13). doi:10.1002/adfm.201808306
43. Qiu M, Singh A, Wang D, et al. Biocompatible and biodegradable inorganic nanostructures for nanomedicine: silicon and black phosphorus. *Nano Today*. 2019;25:135–155. doi:10.1016/j.nantod.2019.02.012
44. Wang X, Li Y, Feng Y, Cheng H, Li D. Macrophage polarization in aseptic bone resorption around dental implants induced by Ti particles in a murine model. *J Periodontal Res*. 2019;54(4):329–338. doi:10.1111/jre.12633
45. Kelleher FC, O'Sullivan H. Monocytes, macrophages, and osteoclasts in osteosarcoma. *J Adolesc Young Adult Oncol*. 2017;6(3):396–405. doi:10.1089/jayao.2016.0078
46. Yamaguchi T, Movila A, Kataoka S, et al. Proinflammatory M1 macrophages inhibit RANKL-induced osteoclastogenesis. *Infect Immun*. 2016;84(10):2802–2812. doi:10.1128/IAI.00461-16
47. Zheng ZW, Chen YH, Wu DY, et al. Development of an accurate and proactive immunomodulatory strategy to improve bone substitute material-mediated osteogenesis and angiogenesis. *Theranostics*. 2018;8(19):5482–5500. doi:10.7150/thno.28315
48. Ma D, Zhang J, Zhang Y, et al. Inhibition of myocardial hypertrophy by magnesium isoglycyrrhizinate through the TLR4/NF-kappaB signaling pathway in mice. *Int Immunopharmacol*. 2018;55:237–244. doi:10.1016/j.intimp.2017.12.019
49. Karfarma M, Esnaashary MH, Rezaie HR, Javadpour J, Naimi-Jamal MR. Poly(propylene fumarate)/magnesium calcium phosphate injectable bone composite: effect of filler size and its weight fraction on mechanical properties. *Proc Inst Mech Eng H*. 2019;233(11):1165–1174. doi:10.1177/0954411919877277
50. Su NY, Peng TC, Tsai PS, Huang CJ. Phosphoinositide 3-kinase/Akt pathway is involved in mediating the anti-inflammation effects of magnesium sulfate. *J Surg Res*. 2013;185(2):726–732. doi:10.1016/j.jss.2013.06.030
51. Schorn L, Sproll C, Ommerborn M, Naujoks C, Kubler NR, Depprich R. Vertical bone regeneration using rhBMP-2 and VEGF. *Head Face Med*. 2017;13(1):11. doi:10.1186/s13005-017-0146-0
52. Cakir-Ozkan N, Egri S, Bekar E, Altunkaynak BZ, Kabak YB, Kivrak EG. The use of sequential VEGF- and BMP2-releasing biodegradable scaffolds in rabbit mandibular defects. *J Oral Maxillofac Surg*. 2017;75(1):221e221–221 e214. doi:10.1016/j.joms.2016.08.020
53. Shui YM, Lv GY, Shan LT, et al. Epimedin C promotes vascularization during BMP2-induced osteogenesis and tumor-associated angiogenesis. *Am J Chin Med*. 2017;45(5):1093–1111. doi:10.1142/S0192415X17500598
54. Carmeliet P. VEGF as a key mediator of angiogenesis in cancer. *Oncology*. 2005;69(Suppl 3):4–10. doi:10.1159/000088478
55. Pan H, Xie Y, Zhang Z, et al. Immunomodulation effect of a hierarchical macropore/nanosurface on osteogenesis and angiogenesis. *Biomed Mater*. 2017;12(4):045006. doi:10.1088/1748-605X/aa6b7c
56. Naito J, Kaji H, Sowa H, Hendy GN, Sugimoto T, Chihara K. Menin suppresses osteoblast differentiation by antagonizing the AP-1 factor, JunD. *J Biol Chem*. 2005;280(6):4785–4791. doi:10.1074/jbc.M408143200
57. Masuda Y, Inami W, Miyakawa A, Kawata Y. Cell culture on hydrophilicity-controlled silicon nitride surfaces. *World J Microbiol Biotechnol*. 2015;31(12):1977–1982. doi:10.1007/s11274-015-1946-7